Brain, Behavior, and Immunity 62 (2017) 265–276

Contents lists available at ScienceDirect

Brain, Behavior, and Immunity

journal homepage: www.elsevier.com/locate/ybrbi

Full-length Article

Maintaining unperturbed cerebral blood flow is key in the study of brain metastasis and its interactions with stress and inflammatory responses

Amit Benbenishty [a,b,c], Niva Segev-Amzaleg [b], Lee Shaashua [c], Rivka Melamed [c], Shamgar Ben-Eliyahu [a,c], Pablo Blinder [a,b,*]

[a] Sagol School of Neuroscience, Tel Aviv University, Israel
[b] Neurobiology Department, George S. Wise Faculty of Life Sciences, Tel Aviv University, Israel
[c] School of Psychological Sciences, Tel Aviv University, Israel

ARTICLE INFO

Article history:
Received 14 November 2016
Received in revised form 8 February 2017
Accepted 16 February 2017
Available online 20 February 2017

Keywords:
Brain
Metastasis
Blood flow
In vivo
Inflammation
Stress
Inoculation method

ABSTRACT

Blood-borne brain metastases are associated with poor prognosis, but little is known about the interplay between cerebral blood flow, surgical stress responses, and the metastatic process. The intra-carotid inoculation approach, traditionally used in animal studies, involves permanent occlusion of the common carotid artery (CCA). Herein we introduced a novel intra-carotid inoculation approach that avoids CCA ligation, namely – assisted external carotid artery inoculation (aECAi) – and compared it to the traditional approach in C57/BL6 mice, assessing cerebral blood flow; particle distribution; blood-brain barrier (BBB) integrity; stress, inflammatory and immune responses; and brain tumor retention and growth. Doppler flowmetry and two-photon imaging confirmed that only in the traditional approach regional and capillary cerebral blood flux were significantly reduced. Corticosterone and plasma IL-6 levels were higher in the traditional approach, splenic numbers of NK, CD3+, granulocytes, and dendritic cells were lower, and many of these indices were more profoundly affected by surgical stress in the traditional approach. BBB integrity was unaffected. Administration of spherical beads indicated that CCA ligation significantly limited brain distribution of injected particles, and inoculation of D122-LLC syngeneic tumor cells resulted in 10-fold lower brain tumor-cell retention in the traditional approach. Last, while most of the injected tumor cells were arrested in extra-cranial head areas, our method improved targeting of brain-tissue by 7-fold. This head versus brain distribution difference, commonly overlooked, cannot be detected using *in vivo* bioluminescent imaging. Overall, it is crucial to maintain unperturbed cerebral blood flow while studying brain metastasis and interactions with stress and inflammatory responses.

1. Introduction

Brain metastases are prevalent in various types of cancer, and are associated with poor prognosis (Kienast and Winkler, 2010; Preusser et al., 2012; Sperduto et al., 2010). To form brain metastases, malignant cells are subjected to physiological processes that are closely dependent on hemodynamics and cerebral vascular structure. Initially, tumor cells must be arrested in the capillary bed of the brain. This process is attributed to specific cell adhesion molecules (Hinton et al., 2010; Lee et al., 2004a,b) and size restrictions (Kienast et al., 2010; Lorger and Felding-Habermann, 2010), and takes place at locations where shear forces are reduced, such as bifurcations of small capillaries (Kienast et al., 2010). Thereafter, arrested cells need to cross the blood-brain barrier (BBB) and extravasate into the brain parenchyma to form brain metastases. Therefore, any experimentally-introduced alterations in cerebral blood flow dynamics, vascular structure, or BBB permeability, might directly hinder our ability to extrapolate findings obtained in such distorted physiological context to the "natural" process of brain metastasis.

Commonly, studies of brain metastasis aiming to study the various steps of the metastatic process, implement one of two intravascular inoculation approaches – (i) intracardiac and (ii) intra-carotid injection. The main disadvantages of the intracardiac injection (Conley, 1979), as reviewed by Daphu et al. (2013), are that (i) tumor cells are distributed from the heart in unknown and uncontrolled proportions to the brain, and (ii) malignant foci develop outside the brain as well. Both of these shortcomings pose

* Corresponding author at: Department of Neurobiology, George S. Wise Faculty of Life Sciences, Sherman Building, Room 419, Tel-Aviv University, Tel Aviv 69978, Israel.
E-mail address: pb@post.tau.ac.il (P. Blinder).

http://dx.doi.org/10.1016/j.bbi.2017.02.012
0889-1591/

substantial obstacles for interpretation of results, and for the study of various factors that may also affect cardiac blood distribution and blood pressure and flow, including surgical procedures (Kirnö et al., 1994), stress (Middlekauff et al., 1997), and a variety of health behaviors (Sullivan et al., 1989; Wilde et al., 2000). The intra-carotid artery (ICAi) inoculation was first described by Machinami (1973). In this approach, cancer cells are injected through the common carotid artery (CCA) into the internal carotid artery (ICA), which provides blood to the brain. However, a small puncture is cut in the artery for the insertion of the injection device, and to avoid consequent bleeding, this procedure necessitates permanent occlusion of the CCA, thus chronically alters blood flow. In more recent versions, the external carotid artery (ECA), which provides blood to peripheral head tissues (including the skull, face, and neck), is also occluded, in order to stream a larger proportion of tumor cells to the brain (Ushio et al., 1977). Due to the structure of the circle of Willis, blood provided by the contralateral ICA reaches both hemispheres of the brain, potentially avoiding severe ischemic conditions. However, acute and chronic changes in tissue oxygen supply may result in profound effects on systemic inflammation and immune activity (Melillo, 2011; Semenza, 2009), which are key mediators of cancer progression (Coussens and Werb, 2002; Dalgleish and O'Byrne, 2006; Grivennikov et al., 2010). We hypothesized that the permanent occlusion of the CCA may have major influences on the complex process of blood-borne brain metastasis and its study under different stress and inflammatory levels. To address this potential limitation, several methods which avoid ligation of the CCA have been recently developed (Chen et al., 2009; Chua et al., 2011; Do et al., 2014). Nevertheless, with respect to brain metastases, no study has been conducted to systematically assesse the significance of maintaining proper blood flow to the brain.

We herein present a novel carotid artery inoculation approach, where tumor cells are administered through the ECA to the ICA, namely – the assisted external carotid artery inoculation (aECAi) approach. The term assisted is derived from the use of a fine positioning device to access the ECA (~200 μm internal diameter), an otherwise a surgical challenge. The aECAi approach has all the advantages of the traditional ICAi method, while completely avoiding occlusion of the CCA. We compared the aECAi to the ICAi approach with respect to perturbations of cerebral blood flow, BBB permeability, stress, inflammatory, and immune responses, blood-borne synthetic particle distribution in the brain (Silasi et al., 2015), and metastatic efficacy and growth. We found our novel approach to avoid the marked distortions of key physiological parameters induced by the ICAi approach, and to result in markedly different outcomes and patterns of metastatic progression in the brain.

2. Materials and methods

2.1. Cell preparation

D122 Lewis Lung Carcinoma (LLC) cells were cultured in complete media (RPMI1640 supplemented with 10% fetal bovine serum and 1% penicillin/streptomycin; Biological Industries). Cells were double labeled with mCherry and Luc2 (pLNT/Sffv-MCS/ccdB plasmid was kindly provided by Prof. Vaskar Saha). For experiments assessing cancer-cell retention, D122 cells were incubated with ^{125}IUDR during the last 24 h of proliferation. Cells were washed and harvested (0.25% trypsin-EDTA; Invitrogen) at ~90% confluence, re-suspended in PBS supplemented with 0.1% BSA (Biological Industries), and kept on ice throughout the injection procedures, completed within 3 h of cell harvesting. More than 95% of cells were vital throughout the injection period.

2.2. Animals and anesthesia

All studies were approved by the institutional IRB committee for animal use and welfare. C57BL/6J male mice were used in all experiments (8–12 weeks old; age matched within experiment). Animals were housed under standard vivarium conditions (22 ± 1 °C, 12 h light/dark cycle, with ad libitum food and water). For anesthesia, mice were first anesthetized in 5% Isoflurane, and then maintained on 1.5–2% throughout the procedures. When anesthetized, core body temperature of animals was maintained at 37 °C.

2.3. Injection procedures

In experiments assessing blood flow and BBB permeability, no cancer cells were injected to avoid potential confounding effects. In experiments assessing organ tumor retention and histological outcomes, $1x10^5$ cells (100 μl) were injected in both methods.

2.3.1. Intra-carotid artery inoculation (ICAi)

The standard protocol was followed (Kienast et al., 2010; Schackert et al., 1989). Mice were anesthetized and restrained in a supine position under a dissecting microscope. The trachea was exposed, and muscles were separated to uncover the right CCA and ECA, which were then separated from the vagus nerve. A 6-0 silk ligature (659, Assut sutures) was tied around the ECA between the superior thyroid artery and the bifurcation of the ECA and CCA (Fig. 1b). A second ligature was loosely placed around the CCA just rostral to the ECA bifurcation, and another ligature was placed and tied further rostral on the CCA. The CCA was then nicked between the two CCA ligatures with a pair of micro-scissors (15000-03, FST), and a stretched polyethylene tube (PE10, Braintree Scientific) fitted on a 100 μl nano-fill syringe (NanoFil-100, WPI) was inserted into the artery lumen and threaded up to the bifurcation of the ligated ECA and the open ICA. Fluid containing the injected material (100 μl) was infused throughout 60sec. The tube was then removed, the loose CCA ligature immediately tightened, and the skin sutured.

2.3.2. Assisted external carotid artery inoculation (aECAi)

Mice were anesthetized and the trachea was exposed similarly to the ICAi method. Thereafter, the sternohyoid muscle was separated, and the ECA uncovered (Fig. 1c). A 6-0 silk-suture ligature was loosely placed around the ECA between the superior thyroid artery and the bifurcation of the ECA and CCA. A second ligature was tied on the ECA distal to the bifurcation, and the ECA was lightly stretched to allow smooth insertion of the needle. A 100 μl nano-fill syringe with a 34G beveled needle was mounted to a micromanipulator (M33, Sutter Inc.). The use of such a device drastically improves success rates and allows standardizing this procedure among laboratories. The needle was inserted slowly into the lumen of the ECA at an angle of ~15° and advanced to the point of bifurcation. The first ligature was tied around the needle, and 100 μl of the fluid containing the injected material was slowly infused throughout 60sec, exactly as in the traditional ICAi approach. The needle was then removed, the ligature quickly tied, and the skin sutured. Notably, use of a micromanipulator is key to the success of this procedure given the delicacy and size of the target vessel (~200 μm internal diameter).

2.4. Awake two-photon laser scanning microscopy

For two-photon microscopy measurements, mice were implanted with a polished and reinforced thin-skull (PoRTS) window, as previously described (Drew et al., 2010). Mice were then

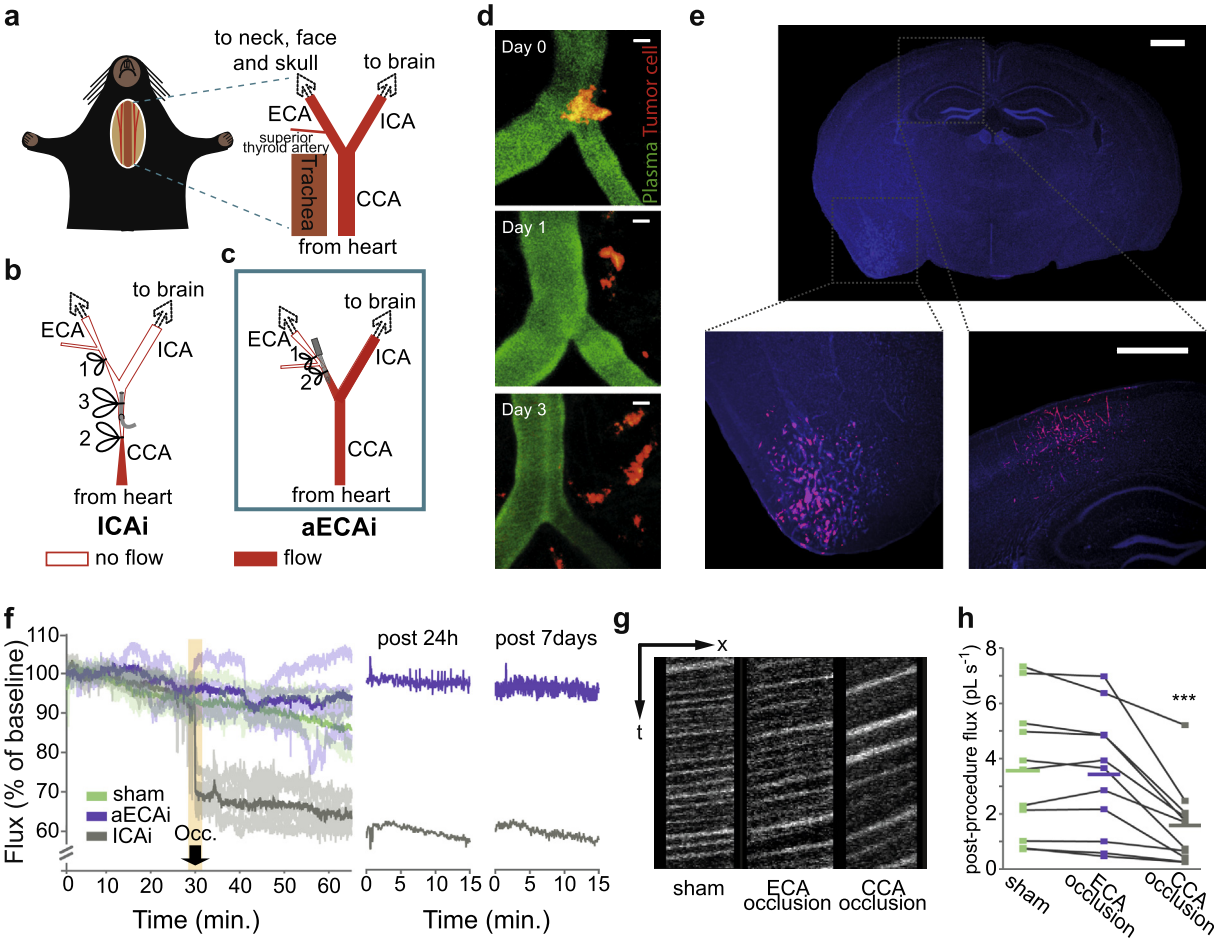

Fig. 1. The novel aECAi approach maintains normal blood flow through the ICA to the brain, as opposed to the traditional ICAi approach. Orientation of the left carotid arteries (a). In the ICAi approach, a small tube or glass cannula is inserted through the CCA, which is then occluded, resulting in permanent cessation of blood flow through the ICA, which supplies the brain (b). In the aECAi approach, a needle is inserted into the ECA, not affecting blood flow through the ICA (c). Numbers in panels (b) and (c) indicate the sequence of permanent ties conducted along the procedures. The cannula/needle is inserted between the last two ties. Inoculation of 1×10^5 LLC-D122 mCherry-Luc cells using the aECAi approach resulted in macro-metastases (14 days following tumor cell injection) (d). Two-photon laser scanning microscopy imaging indicated arrest, extravasation, and beginning of proliferation of tumor cells along the first three days (green – plasma; red – LLC-D122 mCherry-Luc cells) (e). In the ICAi approach (n = 7), regional cerebral blood flow (rCBF), measured by laser Doppler flowmetry, drops significantly (30–40% decrease; $p < 0.001$) (f) immediately after occlusion of the CCA, and remains low for at least 7 days (n = 3). On the other hand, occlusion of the ECA (n = 7) has no effect on rCBF compared to sham (n = 6). In the capillaries, a greater drop is evident (50–60%; $p < 0.001$), as indicated by two-photon laser scanning microscopy. (g) Space-time plots of velocity scans of the same vessel. (h) Calculated flux – mean flux indicated by horizontal lines (n = 12 from three mice in a within-capillary measurement procedure). Scale bars: 10 μm and 1 mm for (d) and (e), respectively. (For interpretation of the references to colour in this figure legend, the reader is referred to the web version of this article.)

habituated to the imaging apparatus for 7 days to reduce procedural stress. Before imaging, mice were injected with 25 μl FITC (5% w/v, i.v.; Sigma-Aldrich) for visualization of the blood plasma. Imaging was conducted with a custom-modified two-photon laser-scanning microscope based on a Sutter MOM (Sutter Inc.) controlled through the MPScope 2.0 software system (Nguyen et al., 2009).

2.5. Quantification of cortical capillary blood flux

In each mouse (n = 3), red blood cells flux was measured in 6–8 capillaries (<8 μm in diameter), using arbitrary scan patterns as previously described (Driscoll et al., 2011), in three time points, sampling the exact same capillaries: (i) following exposure of the trachea (baseline), (ii) 30 min after occlusion of the ECA, and (ii) 30 min after additional occlusion of the CCA. Each of the three imaging sessions lasted approximately 30 min and the entire experiment in each mouse lasted approximately two hours. Procedures for blood flow measurement and analysis have been described previously (Shih et al., 2012).

2.5.1. Imaging of tumor cell extravasation

To verify that tumor cells injected using the aECAi approach extravasate into the brain parenchyma, we imaged the same locations daily for 3 days following tumor-cell administration, and followed mCherry-labeled cells in the brain and their location with respect to blood vessels (Fig. 1d).

2.6. Histology

To demonstrate that the aECAi method is effective in producing brain metastases, mice were injected mCherry-labeled D122 cells. Fourteen days later, animals were transcardially perfused with PBS followed by 4% paraformaldehyde (PFA; EMS). Brains were sliced into 30 μm sections (Leica SM 2000 microtome) and stained with DAPI (MP Biomedicals). Images of the sections were obtained using a fluorescent microscope (SteREO Discovery.V12, Zeiss; Fig. 1e).

2.7. Laser Doppler flowmetry

For measurements of regional cerebral blood flow (rCBF), and the impact of injection procedures on this index, skulls were

thinned above the somatosensory cortex to a depth below the vessels of the bone, avoiding penetration. Thereafter, a metal custom-made probe holder was attached to the skull over the thinned area with dental cement. Mice were then left to recover for one week. rCBF was monitored with a laser Doppler probe (Periflux System 5010, Perimed AB), which was securely screwed to the probe holder to avoid its movement. The Doppler signal was recorded at a sampling rate of 10 kHz, and expressed as percentage of baseline (i.e. average of a 30 min period preceding injection procedures). Injection related alterations in rCBF were assessed from the beginning of the surgical procedure and for 1.5 h. One and seven days later, rCBF was measured again for 15 min. Doppler measurement error was less than 6%, as indicated by repeated measurements within animals (including repeated insertion and exertion of the probe into the custom made holder, and reactivation of the Doppler system, Supplementary Fig. 1a).

2.8. Assessment of BBB permeability

BBB integrity was evaluated, by measuring penetration of a low molecular weight dye, sodium fluorescein (2%; 332 Da; Sigma-Aldrich), as well as a large molecular weight dye, Evans Blue (2%; ~67 kDa when bound to serum albumin; Sigma-Aldrich), as previously described (Kaya and Ahishali, 2011). As positive control, mice were injected with D-mannitol (20%, i.p., Sigma-Aldrich) 15 min preceding dye injection (Lu et al., 2008). For sodium fluorescein assay, mice were sacrificed 30 min following dye administration (Veltkamp et al., 2005), and for Evans Blue assay 24 h after administration (Manaenko et al., 2011). To assess specific brain tissue retention of the dyes, we followed a standard protocol (Kaya and Ahishali, 2011) and analyzed dye content using a spectrophotometer (Mithras LB940; sodium fluorescein – at 530 nm; Evans Blue – at 665 nm).

2.9. Experimental procedure for assessment of corticosterone and immunological factors

Mice were allocated to three groups – non-injected animals, animals injected with 1×10^5 D122-LLC cells using the ICAi approach, and animals injected with tumor cells using the aECAi approach. Half of each group underwent a laparotomy (as previously described (Glasner et al., 2010)), which began just before the injection procedure and lasted for twenty minutes. Twenty-four hours later animals were sacrificed by an overdose of isoflurane, and 0.5 ml of blood was withdrawn by cardiac puncture into syringes containing EDTA (1.8 mg/ml blood; Sigma-Aldrich), centrifuged at 2000 rpm for 20mins, and plasma was stored at −80 °C. Simultaneously, spleens were harvested, grinded in 2.5 ml of PBS and filtered, yielding single-cell suspensions. Fifty μl of cell suspension was then used for FACS analysis (see below).

2.10. Measurement of plasma corticosterone and IL-6

Quantitative enzyme-linked immunosorbent assays (ELISA) were used to quantify corticosterone (AssayMax™ Corticosterone, Assaypro) and IL-6 (900-TM50, PeproTech) levels, as per the manufacturers' instructions.

2.11. Fluorescence activated cell scanner (FACS)

FACS analysis was used to assess the number of NK cells, CD3 positive cells, granulocytes, and dendritic cells in the spleen. Standard procedures were used to prepare cells for FACS analysis (Melamed et al., 2005). NK cells were identified using FITC-conjugated anti-mouse NK1.1 (11-5941, eBioscience), CD3 positive cells were identified by PE-Cy5-conjugated anti-mouse CD3e (15-0031, eBioscience), granulocytes were identified by APC-eFluor 780-conjugated anti-mouse Ly-6G (Gr-1; 47-5931, eBioscience), and dendritic cells were identified by PE-conjugated anti-mouse 33D1 (12-5884, eBioscience). Flow cytometry analysis was conducted using a FACScan (Becton Dickinson). To assess the total number of cells per μl of spleen suspension, 300 polystyrene microbeads per μl of sample (20 μm diameter; 9020; Duke Scientific) were added to each sample. Following cytometry, the formula: (# events per cell population/# microbead events) × 300 was used to calculate the number of cells per microliter sample. The coefficient of variation for this method in our laboratory was found to be 6% or less for identical samples.

2.12. Assessment of blood distribution using fluorescent beads

In order to assess the potential of cancer cells injected employing the two different approaches to reach and arrest in different regions of the brain, 5×10^4 10 μm eGFP-tagged spherical latex beads (F8836, ThermoFisher Scientific) were injected. One hour later, mice were sacrificed and brain, lungs, liver, and kidney were collected and fixated in 4% PFA (EMS) over night. Images of whole tissue were obtained using a fluorescent microscope (SteREO Discovery.V12, Zeiss). Notably, of the peripheral organs, beads were evident only in the lungs. Brains were then sliced into 100 μm sections using a microtome, and the number of beads/tissue volume was quantified using FIJI software (version 2.0.0-rc-43/1.50e).

2.13. Brain and peripheral organ retention of cancer cells

Mice were injected with 1×10^5 ^{125}IUDR labeled D122-LLC cells using either the ICAi or the aECAi approach, and euthanized 24 h later. Animals were divided into two groups – one of which was transcardially perfused with 20 ml PBS supplemented with 30U heparin (Sigma-Aldrich), and another which was not perfused. Right and left brain hemispheres, lungs, and liver were collected from the perfused animals, extra-cranial head tissue was additionally collected from the non-perfused animals, and radioactivity in each organ was measured using a gamma counter (2470, PearkinElmer).

2.14. Bioluminescent imaging

In vivo bioluminescent imaging using an IVIS SpectrumCT (PearkinElmer) was performed in anesthetized mice injected with D122-mCherry-Luc2 cells. Imaging sessions were conducted at 15 min (t0), and 1, 4, 7, and 14 days following tumor cell administration. After the last *in vivo* imaging session, mice were sacrificed, and brain and extra-cranial head tissue were rapidly imaged separately. Each imaging session was preformed between 10-20 min. following D-Luciferin sodium salt injection (30 mg/ml, 100 μl, i.p; Regis Technologies), as this time frame exhibited maximal and steady intensity. Analysis was done using Living Image software (version 4.3.1).

2.15. Statistical analysis

SPSS (version 23.0) was used to perform statistical tests (*t*-test or ANOVA, with the Bonferroni correction for multiple post hoc comparisons). p-values less than 0.05 were considered statistically significant. All data are presented as mean ± SEM. $^{*}p < 0.05$; $^{**}p < 0.01$; $^{***}p < 0.001$. If not specified otherwise, sample size (n) refers to number of mice.

3. Results

3.1. Occlusion of the CCA markedly reduced cerebral blood flow

Using laser Doppler flowmetry, we measured the effects of the inoculation methods on rCBF. In the ipsilateral hemisphere, the ICAi method resulted in a significant 30–40% drop in rCBF compared to baseline measurements ($F_{(2,14)} = 79.469$, $p < 0.0001$), to sham operated mice ($p < 0.0001$), and to aECAi operated animals ($p < 0.0001$). In contrast, the aECAi method had exerted no impact on rCBF (Fig. 1f). The drop in blood flux is attributed to the occlusion of the CCA, as it always occurred immediately when the CCA was ligated. No other procedure during the surgeries resulted in significant or permanent changes in rCBF, including the occlusion of the ECA and inoculation with saline. To assess whether this drop persists, rCBF was measured again at 24 h and 7 days after inoculation. rCBF remained significantly low in the ICAi method (24 h – $F_{(2,6)} = 112.044$, $p < 0.001$; 7 days – $F_{(2,6)} = 130.280$, $p < 0.001$) and stable in the aECAi method at both time points (Fig. 1f), indicating that the reduction is permanent. When blood flow was measured in the contralateral hemisphere, no change was apparent in either inoculation method (supplementary Fig. 1b).

An even more drastic drop in blood flux was observed in cerebral capillaries, following CCA occlusion, as measured using two-photon microscopy. Occluding only the ECA did not affect capillary blood flux, whereas additional occlusion of the CCA resulted in a 60% drop in the ipsilateral hemisphere ($t(10) = 9.617$, $p < 0.0001$; Fig. 1g–h).

3.2. BBB permeability was unaffected by either inoculation approach

Next, we measured the effects of the inoculation approach on the integrity of the BBB, using the Evans Blue and sodium fluorescein assays. In both hemispheres no sign of BBB breakdown was evident in neither of the inoculation approaches 2 and 24 h after inoculation, while mice injected with mannitol (positive control) exhibited increased BBB permeability in both assays (Evans Blue – $F(3,6) = 28352.906$, $p < 0.001$; sodium fluorescein – $F(3,6) = 1057.042$, $p < 0.001$) (supplementary Fig. 2).

3.3. Occlusion of the CCA resulted in lower number and limited distribution of particles in the brain tissue

To test whether the inoculation approach affects potential distribution of cancer cells to the brain, 10 μm fluorescent latex

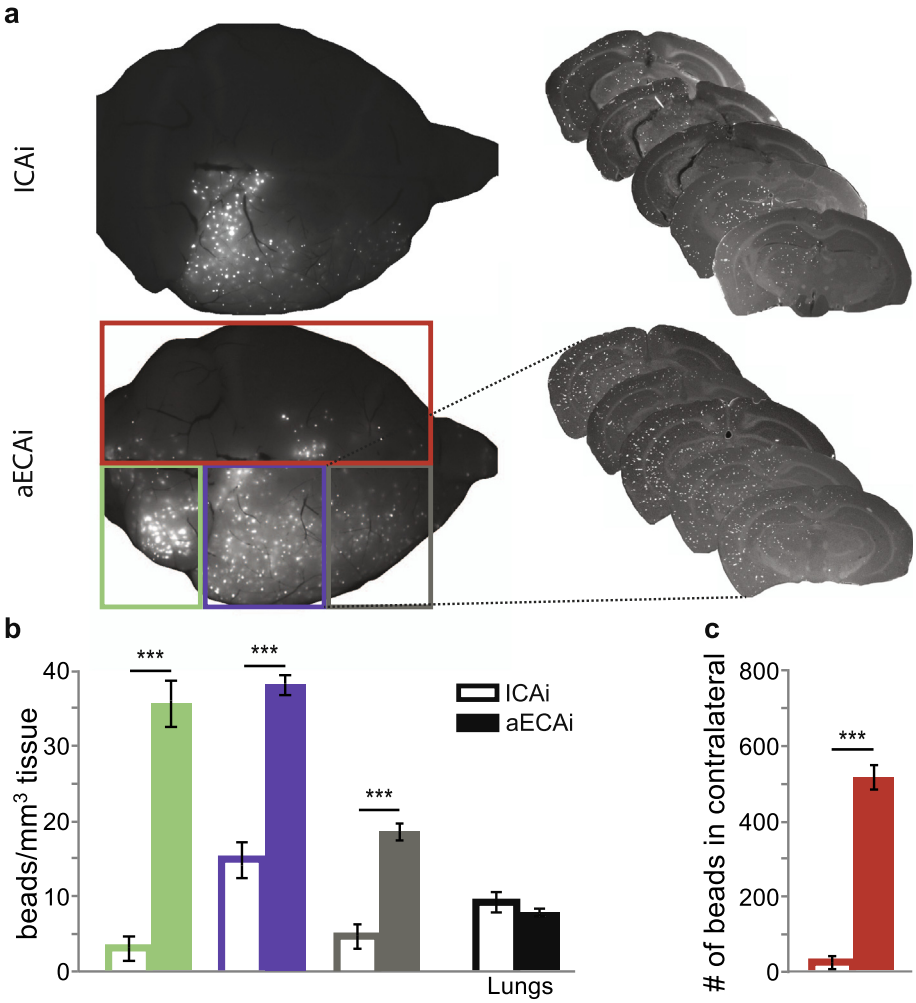

Fig. 2. The novel aECAi approach results in a higher numbers of arrested beads in the brain, with a greater distribution area, compared to the traditional ICAi approach. Representative images of whole brains, which were sliced (100 μm coronal sections) for localization and quantification of fluorescent beads (a). In both approaches (n = 4), the greatest portion of beads within the brain were located in the medial region (purple rectangular/bars; Bregma to Bregma-5 mm; $p < 0.001$). Importantly, in all regions, including the ventral (green rectangular/bars; Bregma-5 mm to Bregma-8 mm), medial, and rostral (grey rectangular/bars; Bregma to Bregma + 3 mm) regions of the brain, significantly more beads were arrested when using the novel aECAi approach ($p < 0.001$) (b). A profound difference was also evident in the contralateral hemisphere, where almost no beads were detected in the ICAi approach (red rectangular/bars; $p < 0.001$) (c). In contrast, there was no difference in the arrest of beads in the lungs (b). (For interpretation of the references to colour in this figure legend, the reader is referred to the web version of this article.)

beads were injected (Silasi et al., 2015). The standard ICAi approach yielded 3-fold lower levels of beads arrested in the brain compared to the aECAi approach ($t(6) = 21.387$, $p < 0.001$), while no differences in peripheral organs beads retention were evident (Fig. 2b). When using the novel aECAi approach, beads were distributed throughout regions supplied by the medial and anterior cerebral arteries in the ipsilateral hemisphere (dorsolateral frontal lobe, the anterior superior temporal lobe, and the frontoparietal area). Interestingly, in the contralateral hemisphere almost no beads were evident using the ICAi approach, while a significant amount was evident in the aECAi approach in the region supplied by the contralateral anterior cerebral artery (Fig. 2c). In both cases, the majority of beads arrested in the brain were found in the medial region of the ipsilateral hemisphere (Bregma to Bregma-5 mm), an area that is supplied by the middle cerebral artery – the main upstream branch of the ICA (Fig. 2b).

3.4. Occlusion of the CCA resulted in elevated plasma corticosterone levels

To test whether occlusion of the CCA results in elevated stress levels, plasma corticosterone was measured 24 h post-surgery in mice undergoing ICAi, aECAi, or no injection, with or without an additional surgical procedure (i.e. laparotomy). Injection approach significantly altered corticosterone levels ($F_{(2,41)} = 8.612$, $p = 0.001$). Specifically, post hoc analysis indicated that animals subjected to the ICAi approach exhibited higher corticosterone levels compared to animals undergoing aECAi ($p = 0.021$) and compared to control animals ($p = 0.001$), while no significant difference was evident between the aECAi and control animals ($p = 0.784$). In non-laparotomized animals undergoing ICAi, plasma corticosterone levels were higher compared to control animals ($p = 0.015$), while aECAi did not have such an effect ($p = 0.271$). Within animals undergoing laparotomy, corticosterone levels were significantly higher in the ICAi approach compared to either aECAi ($p = 0.011$) or control animals ($p = 0.005$), and no difference was evident between the aECAi and control animals ($p = 0.624$) (Fig. 3a).

3.5. Occlusion of the CCA resulted in elevated IL-6 plasma levels

To test whether occlusion of the CCA results in systemic inflammation, plasma IL-6 was measured 24 h post-surgery (injection and/or laparotomy). While Surgery did not affect plasma IL-6 levels in either group at this time point ($F_{(1,15)} = 0$; $p = 0.996$), the injection approach did ($F_{(2,15)} = 5.399$, $p = 0.017$). ICAi animals exhibited higher levels of IL-6 than aECAi animals ($p = 0.029$), and marginally significant higher levels than control animals ($p = 0.062$). In non-laparotomized animals, IL-6 levels were approximately 4–5 times higher when using the ICAi approach compared to control animals ($p = 0.043$) and animals that underwent aECAi ($p = 0.045$) (Fig. 3b).

3.6. Occlusion of the CCA resulted in reduced immune cells numbers in the spleen, a phenomena augmented by surgery

The different injection approaches resulted in altered numbers of splenic leukocyte subpopulation, including NK cells ($F_{(2,15)} = 5.572$, $p = 0.016$), CD3+ cells ($F_{(2,15)} = 8.246$, $p = 0.004$), granulocytes ($F_{(2,15)} = 5.678$, $p = 0.015$), and dendritic cells ($F_{(2,15)} = 3.850$, $p = 0.045$), and laparotomy resulted in reduced NK cells ($F_{(1,15)} = 7.277$, $p = 0.017$) and granulocytes ($F_{(1,15)} = 4.700$, $p = 0.047$). Specifically, post hoc analyses indicated that animals undergoing ICAi had reduced numbers of NK cells ($p = 0.016$), CD3+ cells ($p = 0.004$), granulocytes ($p = 0.014$), and dendritic cells ($p = 0.043$) compared to control, and reduced CD3+ cells compared to aECAi animals ($p = 0.048$). The aECAi approach did not significantly reduce number of splenocyte subpopulations. In non-laparotomized animals, ICAi resulted in reduced NK cells compared to control and compared to aECAi, while the aECAi approach had no such impact (Fig. 3c).

3.7. Occlusion of the CCA reduced tumor cell arrest and infiltration in the brain and enhanced extra-cranial head tumor retention

Tumor retention analysis of brains, which underwent perfusion 24 h after inoculation, revealed an enhanced brain arrest and/or infiltration of ^{125}IUDR-labeled D122 cancer cells when injected with the aECAi method compared to the ICAi method (Fig. 4a). This difference was evident in both hemispheres, with a larger effect in the ipsilateral hemisphere ($t(6) = 4.581$, $p = 0.004$). Notably, in the ICAi method, signals from the contralateral hemispheres were at zero level, recapitulating the observed distribution of latex beads. Tumor cells that pass through the brain flow through the heart to the lungs, and thereafter to other peripheral organs. Assessing these peripheral organs, we observed no difference between the two methods (Fig. 4a). Importantly, and given the differences observed in the brain tissue, in the ICAi method, there were ~4-fold more cancer cells retained in the lungs and ~6-fold more in the liver than in the brain, while in the aECAi approach, the brain was the organ with the highest retention ($F_{(3,24)} = 8.827$, $p < 0.001$; Fig. 4a).

Because peripheral organs showed similar retention levels, while brains showed markedly reduced retention levels in the ICAi approach, we suspected that the "missing" cells are located in head areas outside the brain, that are also supplied by the CCA. To test this prediction, radioactive tumor retention was measured separately in brains and extra-cranial head tissue. In both inoculation approaches there were significantly more cancer cells retained in the head compared to the brain (ICAi – $t(10) = 6.863$, $p < 0.001$, aECAi – $t(8) = 2.958$, $p = 0.018$), but the proportion of head/brain was 7-fold greater in the ICAi approach compared to the aECAi approach ($t(9) = 2.624$, $p = 0.028$; Fig. 4b), indicating that the missing cells were indeed located in the head area.

3.8. The effects of inoculation technique on tumor retention and metastatic growth in bioluminescent imaging

Whole animal bioluminescent imaging does not allow distinguishing between brain and extra-cranial head tissues that bear live tumor cells. Indeed, there were no differences in bioluminescence between the inoculation approaches immediately after inoculation and at 24 h later (Fig. 4d). In both approaches, bioluminescence signaling decreased between the inoculation time and 24 h following it (aECAi – $t(4) = -5.387$, $p = 0.006$; ICAi – $t(4) = -5.185$, $p = 0.007$), indicating tumor cell clearance from the brain/head area. From 4 to 7 to 14 days following inoculation, tumor burden in the brain/head increased (becoming significant at day 7 for the ICAi approach ($p = 0.001$), and at day 14 for the aECAi approach ($p < 0.001$)), reflecting proliferation of cancer cells. At 4 and 7 days after inoculation, there was a greater signal in mice inoculated using the ICAi approach ($F_{(1,8)} = 8.325$, $p = 0.020$ and $F_{(1,8)} = 19.893$, $p = 0.002$, respectively; Fig. 4d), and this difference dissipated on day 14 post-inoculation, when mice were sacrificed. *Ex-vivo* imaging of the brain and head revealed no differences between the methods, however, it demonstrated that there was a stronger signal (indicating metastatic burden) in the extra-cranial head tissue compared to the brain itself, in both administration approaches (Fig.4e; ICAi – $t(4) = 3.488$, $p = 0.025$; aECAi – $t(4) = 3.704$, $p = 0.021$).

4. Discussion

Brain metastases are often lethal, and prophylactic and therapeutic treatments are scant (Kienast and Winkler, 2010; Preusser

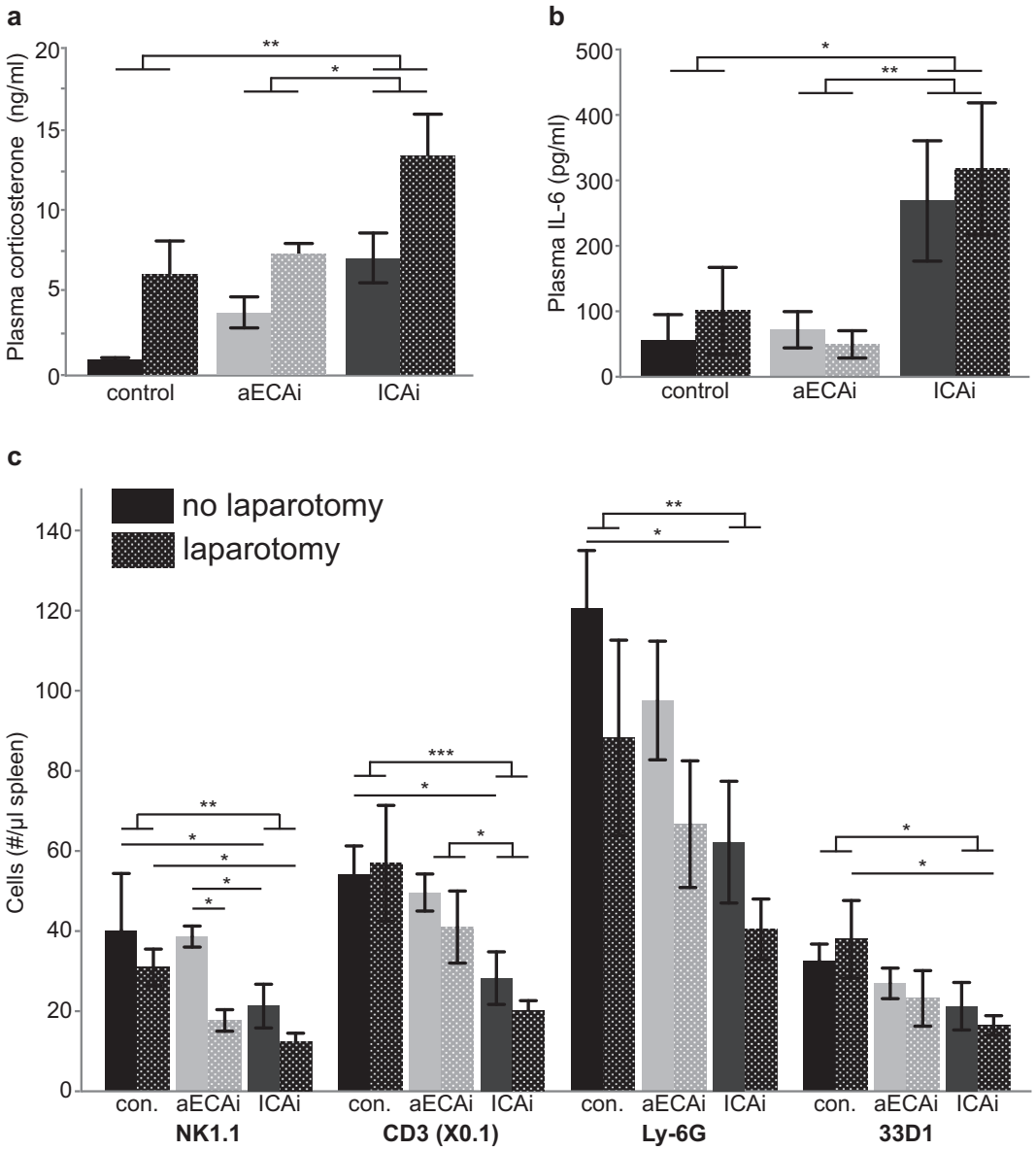

Fig. 3. The traditional ICAi approach results in elevated corticosterone levels, higher levels of plasma IL-6, and reduced numbers of various splenocyte subtypes. The ICAi approach resulted in higher corticosterone (a) and higher IL-6 (b) levels compared to both the aECAi approach and control conditions, while the aECAi approach did not differ significantly from control condition. Animals undergoing ICAi had reduced numbers of NK cells, CD3+ cells, granulocytes ($p = 0.014$), and dendritic cells compared to control, and reduced CD3+ cells also compared to aECAi animals. The aECAi approach did not significantly reduce number of splenocyte subpopulations. In non-laparotomized animals, ICAi resulted in reduced NK cells compared to control and compared to aECAi, while the aECAi approach had no such impact (c).

et al., 2012; Sperduto et al., 2010), apparently due to limited understanding of the mechanisms that regulate metastatic efficacy in the brain. Common obstacles in using animal models to study brain metastasis are methodological artifacts that limit the validity of the outcomes and their generalizability to the clinical setting. Specifically, injection procedures may alter cerebral blood flow, blood distribution, vascular structure or permeability, or stress and immune-inflammatory indices. Given that brain metastases originate from circulating malignant cells that reach the brain through its vasculature, and cross the BBB to colonize it, any such perturbations introduce experimental artifacts. In order to address this limitation, we developed the aECAi approach that avoids impeding blood flow to the brain. In the present study, we show that the traditionally used injection approach, in which the CCA is occluded, has profound undesirable effects on cerebral blood flow, and results in reduced particle distribution in the brain. Moreover, the traditional approach has vast effects on stress levels and systemic immune parameters, alone, and when employed in the context of an extensive surgery. Last, the traditional inoculation approach reduced retention of tumor cells in the brain, and enhanced retention in extra-cranial head tissue. In contrast, the method presented herein maintains normal blood flow and immune-inflammatory status, thereby better preserves physiological conditions, enabling more clinically-relevant studies of brain metastasis in various experimental settings.

Specifically, cessation of blood flow through the CCA resulted in a significant and permanent drop in regional (30–40%) and capillary (60%) cerebral blood flow in the ipsilateral hemisphere (Fig. 1). Reduction of a similar degree (20–40% in rCBF) has been shown by others to result in multiple infarcts, and in motor impairments and behavioral changes four weeks following bilateral constriction of the CCAs (Hattori et al., 2015). Thus, in addition to

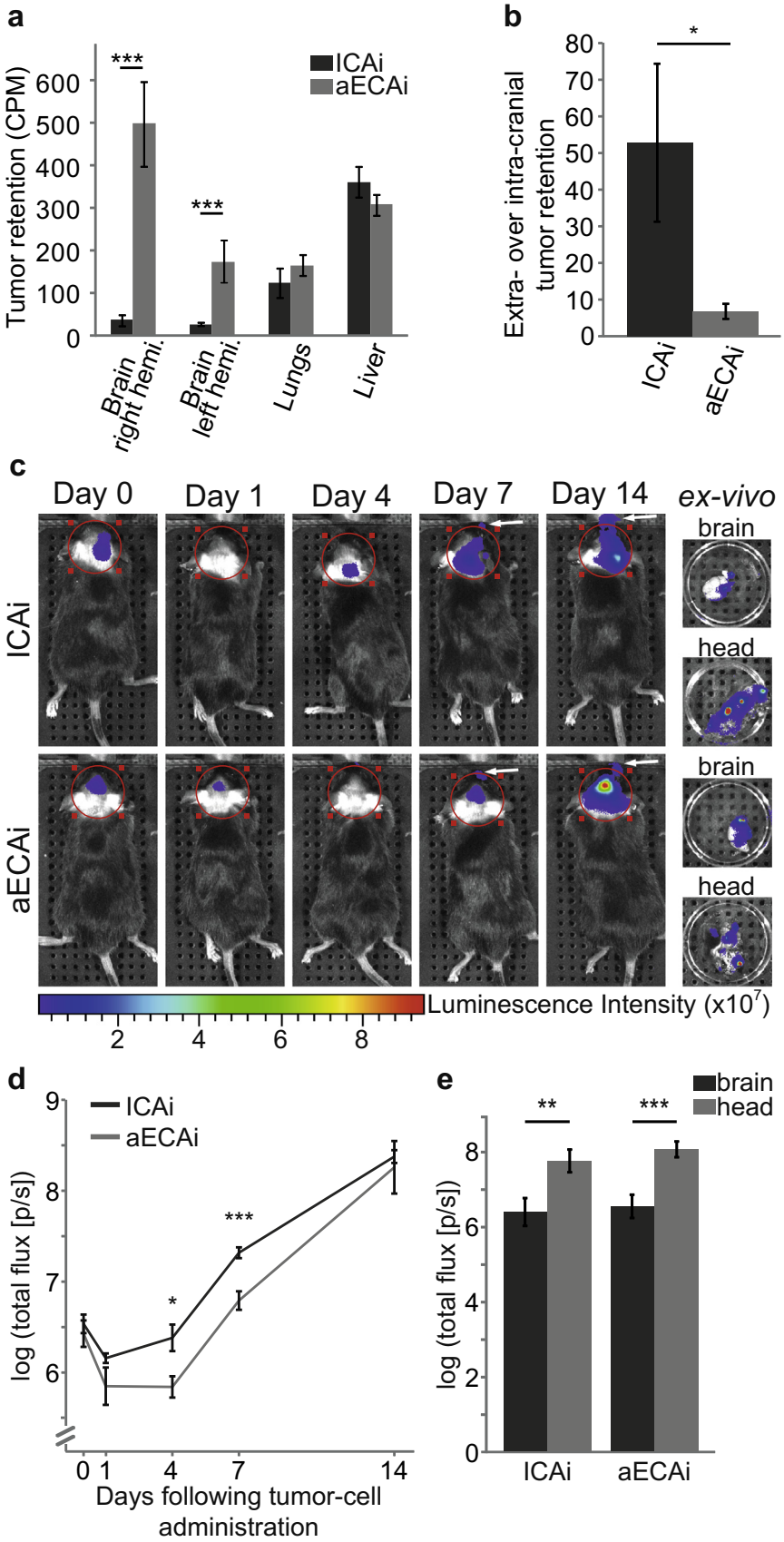

Fig. 4. The traditional ICAi approach results in reduced tumor-cell retention in the brain compared to the novel aECAi approach, and a significantly higher ratio of retention in extra-cerebral over intra-cerebral tissue. Injection of 1×10^5 LLC-D122 mCherry-Luc cells, using the traditional ICAi approach resulted in reduced retention in the brain 24 h following tumor cell administration (n = 8, $p < 0.001$) (a), but enhanced retention in the extra-cranial head tissue (and enhanced extra- to intra-cerebral ratio) compared to the aECAi approach ($p < 0.05$) (b). As would be expected, *in vivo* bioluminescent imaging (c–d), which reflects tumor-derived photon emission from both brain and extra-brain head tissue, revealed no signal differences between the administration approaches immediately following tumor inoculation. At later time points, differences reflect different rates of tumor clearance and tumor proliferation rates between the two injection approaches in the different head/brain compartments. White arrows (c) indicate signals that clearly originate from extra-cranial head tissue. In both approaches, on day 14 post tumor administration, ex-vivo measurements (physically separating brain from extra-brain head tissue) revealed higher signals in extra-cranial head tissue compared to the brain (ICAi – $p < 0.01$; aECAi – $p < 0.001$) (e).

immediate perturbations in blood flow and distribution, numerous brain functions are likely to be compromised in animals subjected to CCA occlusion. Additionally, it is well acknowledged that reduced blood flow can result in compromised BBB integrity (Li et al., 2015). In our study, although a marked drop in blood flow had occurred, no effects on BBB permeability in the first 24 h were evident, with or without CCA occlusion. The absence of BBB breakdown in the first 24h time frame does not contradict existing literature, which reported compromised BBB integrity under ischemic conditions when rCBF decreases by approximately 70–80% (Kraft et al., 2013), whereas in our study CCA occlusion resulted in approximately 30–40% decrease in rCBF.

We also assessed differences between the two approaches with respect to their systemic stress and immune-inflammatory responses, and their interaction with additional surgical trauma. Occlusion of the CCA alone resulted in an approximately sevenfold elevation in corticosterone levels (Fig. 3a), not evident in the aECAi approach (CCA intact). Others and we have reported that systemic stress responses affect multiple indices of metastases initiation and progression in various organs (Cole et al., 2015; Horowitz et al., 2015), including the brain (Rozniecki et al., 2010; Theoharides et al., 2008). Additionally, the traditional ICAi approach resulted in augmented systemic inflammation (i.e. elevated plasma IL-6 levels; Fig. 3b), and previous studies have shown that elevated inflammation, specifically IL-6 (Chang et al., 2013), affects tumor growth, invasion, and metastasis (Joyce and Pollard, 2009; Wu and Zhou, 2009). Last, the traditional, but not the novel aECAi, approach resulted in reduced splenocytes numbers (NK, CD3+, granulocytes, and dendritic cells; Fig. 3c), which indicate immunocytes trafficking or augmented leukocyte apoptosis (Bronte and Pittet, 2013). While the direct effects of this reduction in splenocytes number has not been addressed in the current study, it is acknowledged that such immune perturbations may have profound effects on tumor and metastasis progression, and on therapeutic interventions (Candeias and Gaipl, 2016; Dhabhar et al., 2012; Gotlieb et al., 2015; Melamed et al., 2010). Moreover, while the addition of laparotomy affected animals undergoing aECAi in a pattern similar to the effects evident in non-injected animals, in ICAi operated animals, laparotomy had diverse, often an exaggerated response, compared to control and aECAi operated animals. Taken together, these findings suggest that our novel approach is advantageous for studying the effects of stress or of immune-altering paradigms on brain metastasis.

To form brain metastases, circulating cancer cells must first (i) reach the brain, (ii) arrest in the capillary bed of the brain, and (iii) extravasate into the brain tissue. In this study we showed that spherical latex beads of similar size to cancer cells (10 μm) are arrested throughout the brain with a significantly greater spread when injected using the novel aECAi approach (CCA intact) compared to the traditional ICAi approach (CCA occluded; Fig. 2). These more limited brain areas correspond well with probabilistic maps of ICA blood distribution (J. S. Lee et al., 2004a,b). Moreover, when the CCA was occluded, almost no beads were observed in the contralateral hemisphere. We attribute this phenomenon to the unidirectional blood flow through the Circle of Willis, which may prevent beads from crossing to the contralateral hemisphere. Overall, such unnatural and limited distribution of blood, which carries and spreads malignant cells, may distort processes of cancer metastasis that are location-specific and are affected by flow kinetics, blood pressure, and stress responses (Horowitz et al., 2015; Pein and Oskarsson, 2015). We also found that while there was no difference in the periphery (i.e., lungs), the total number of beads arrested in the brain was ~3-fold lower when the CCA was occluded, which may be related to reduced arrest efficacy in the brain, and/or to distribution of beads to areas within the head, but outside the brain.

To study these processes in a more biologically- and clinically-related manner, and to evaluate the effects of CCA occlusion, we injected syngeneic LLC-D122 tumor cells using both approaches, and 24 h following administration assessed their exclusive retention in each hemisphere of the brain, in the head, and in peripheral organs of the body. Metastatic efficacy in the brain tissue was reduced by ~10-fold when tumor cells were administered in the traditional ICAi approach compared to our aECAi approach, while in the extra-cranial head areas an opposite pattern arose. In contrast, no significant differences in tumor retention were evident in peripheral organs (Fig. 4a), after tumor passage through the brain vasculature. Thus, these results further support our hypothesis that reduced blood flow to the brain alters tumor cells distribution pattern (head vs brain) and decreases the arrest potential of cancer cells in the brain parenchyma. It is well acknowledged that the growth of a tumor in one body compartment may have systemic effects, modulating the growth of other tumor foci (Benzekry et al., 2014; DeWys, 1972). Therefore, studies focusing on metastatic processes within the brain should favor an injection approach that delivers tumor cells more exclusively to brain areas, as in the aECAi.

We also conducted longitudinal *in vivo* bioluminescent imaging, which indicates total tumor burden in a given region of interest, focusing our attention on the head area (including the brain). Given the opposite pattern of differences within and outside the brain, one may expect no differences between the two administration approaches, as indeed were evident immediately after inoculation of cancer cells (within 5–10 min). To verify tumor growth outside the brain tissue, we also separately imaged brains and head areas following euthanization of animals. Indeed, our results indicated marked tumor growth both within and outside the brain tissue, as expected given the 24 h tumor retention outcomes which indicate seeding of tumor cells in both locations. Our results also indicate that, irrespective of tumor administration approach, but more profoundly in the traditional approach, tumor burden was lower in the brain compared to the rest of the head tissue, in both the 24 h tumor retention index and the 14 days bioluminescence index. This observation has crucial implications for *in vivo* bioluminescent imaging of brain metastases (Chung et al., 2009; Du Four et al., 2015; Song et al., 2009; Wolff et al., 2015), which cannot distinguish between cerebral and extra-cerebral signaling. It implies that *ex-vivo* analyses of separated tissues, as conducted herein, have a significant added value. Notably, while cancer cells flow through the ICA that supplies the brain (in both administration approaches), they can also reach tissue outside the cerebrum through anastomoses of the ICA (Figueiredo et al., 2012; Taveras et al., 1954) and its extra-cerebral branches (e.g. ophthalmic artery), and through clearance to the sinuses located within the dura matter outside the brain parenchyma. Interestingly, after 14 days, tumor burden was similar in the ICAi approach compared to the aECAi approach as indicated by ex-vivo imaging, in both the cerebral and extra-cerebral compartments. Given that bioluminescence signaling significantly differed between the inoculation approach in days 4 and 7, we suggest that these differences in tumor growth dynamics result from the different microenvironment characteristics (Fidler, 2011; Joyce and Pollard, 2009; Quail and Joyce, 2013; Zhang and Yu, 2011), including blood flow dynamics, and the initial tumor burden observed by our retention assay (Fig. 4a–b).

Recently, a few similar approaches in which the CCA is not permanently ligated have been suggested for arterial inoculation of substances directed to the brain. In one approach it has been shown that inoculation of stem cells for treatment of stroke, using the traditional ICAi method, resulted in a significant reduction in cerebral blood flow in rats (Chua et al., 2011), similar to our findings in mice. The study also reported that the drop in cerebral

blood flow resulted in micro-infarcts, neuronal damage, and inflammation in the brain. Moreover, when using a micro-needle inoculation, which avoids occlusion of the CCA, these detrimental effects were circumvented. In humans, narrowing of an ICA (located downstream to the CCA) beyond 70% is associated with cognitive impairments, which are reversible by improving perfusion (Yoshida et al., 2015). These findings further support our claim that experimentally-related reduction in ICA blood flow may constitute a significant confound for extrapolating experimental findings regarding brain processes to the clinical setting.

In mice, a chronic cannulation of the ECA was reported and is used for tumor cell inoculation (Chen et al., 2009), but unfortunately this technique was not compared to the traditional ICAi approach, and the importance of unchanged blood flow through the CCA was not assessed. While this procedure does not involve a permanent CCA ligation, a temporary occlusion is necessary, and the procedure is more challenging and involves higher risk for blood loss and mortality compared to the aECAi approach introduced herein. Moreover, this procedure requires 1–2 h to conduct, while in our hands the aECAi is completed within 10–15 min. Procedural timing is critical, as prolonged anesthesia increases morbidity and mortality rates (Grimm et al., 2011), and was suggested to have acute and chronic effects on brain function (Liu et al., 2014). Another approach employed to avoid cessation of blood flow through the CCA is to apply pressure to the artery (Do et al., 2014). However, this approach results in inevitable blood loss and in a high mortality rate.

Integrating our findings, we suggest that the occlusion of the CCA and the consequent drop in blood flow in the ICAi approach underlies all other outcomes in our study. We verified that the same number of tumor cells is injected, and the only technical difference between the two approaches is the ligation of the CCA. Altered blood flow immediately follows, with no other probable direct procedural variations. This drop in blood flow can directly influence particle distribution in the brain and surrounding tissues (Lee et al., 2004a,b), can alter arrest pattern through changes in shear forces and clearance (Kienast et al., 2010), and can indirectly affect tumor cell survival (Hori et al., 1999), extravasation (Strell and Entschladen, 2008), and proliferation through a variety of physiological perturbations, including systemic neuroendocrine responses (Ben-Eliyahu, 2003; Sawchenko and Swanson, 1981), immune activity (Degen and Palumbo, 2012), oxidative stress (Brown and Bicknell, 2001), and inflammation (Harris et al., 2010; Horowitz et al., 2015). Thus, permanent ligation of the CCA, as shown here, has profound effects on the metastatic process in the brain, and may hinder the ability to extrapolate findings to the clinical setting.

Overall, the aECAi approach we developed is advantageous for studying experimental brain metastasis as it (i) has no impact on blood flow to the brain or on BBB integrity, (ii) has a success rate of more than 95% and negligible mortality rate, (iii) induces relatively minor tissue damage and no blood loss, and (iv) inflicts minimal perturbations in stress, immune, and inflammatory indices. This approach results in higher metastatic efficacy in the brain compared to the traditional ICAi approach. Therefore, the aECAi approach bears a greater biological and clinical relevance, especially when studying factors that alter hemodynamic and immune-inflammatory parameters, or that would be affected by such alterations.

Acknowledgments

AB, SBE and PB would like to thank Dr. Eyal Dor-On and Dr. Chen Luxenburg for their help in the generation of the D122-mCherry-Luc2 cell line, and Prof. Avraham Mayevsky for his help with Doppler measurements. AB and PB would like to thank Dr. Andy Shih for his valuable advice during the early stages of the project. AB would like to thank Prof. David Kleinfeld for training in two-photon microscopy in his laboratory. AB is grateful to Dante family and Sagol School of Neuroscience of Tel Aviv University for the award of doctoral fellowship. This work was supported by NIH/NCI grant # CA172138 (SBE) and by the Israeli Science Foundation grant # 1019/15 (PB).

Appendix A. Supplementary data

Supplementary data associated with this article can be found, in the online version, at http://dx.doi.org/10.1016/j.bbi.2017.02.012.

References

Ben-Eliyahu, S., 2003. The promotion of tumor metastasis by surgery and stress: immunological basis and implications for psychoneuroimmunology. Brain Behav. Immun. 17 (Suppl 1), S27–S36.

Benzekry, S., Gandolfi, A., Hahnfeldt, P., 2014. Global dormancy of metastases due to systemic inhibition of angiogenesis. PLoS One 9, e84249. http://dx.doi.org/10.1371/journal.pone.0084249.

Bronte, V., Pittet, M.J., 2013. The spleen in local and systemic regulation of immunity. Immunity 39, 806–818. http://dx.doi.org/10.1016/j.immuni.2013.10.010.

Brown, N.S., Bicknell, R., 2001. Hypoxia and oxidative stress in breast cancer. Oxidative stress: its effects on the growth, metastatic potential and response to therapy of breast cancer. Breast Cancer Res. 3, 323–327.

Candeias, S.M., Gaipl, U.S., 2016. The immune system in cancer prevention, development and therapy. Anticancer. Agents Med. Chem. 16, 101–107.

Chang, Q., Bournazou, E., Sansone, P., Berishaj, M., Gao, S.P., Daly, L., Wels, J., Theilen, T., Granitto, S., Zhang, X., Cotari, J., Alpaugh, M.L., de Stanchina, E., Manova, K., Li, M., Bonafe, M., Ceccarelli, C., Taffurelli, M., Santini, D., Altan-Bonnet, G., Kaplan, R., Norton, L., Nishimoto, N., Huszar, D., Lyden, D., Bromberg, J., 2013. The IL-6/JAK/Stat3 feed-forward loop drives tumorigenesis and metastasis. Neoplasia 15, 848. http://dx.doi.org/10.1593/neo.13706.

Chen, L., Swartz, K.R., Toborek, M., 2009. Vessel microport technique for applications in cerebrovascular research. J. Neurosci. Res. 87, 1718–1727. http://dx.doi.org/10.1002/jnr.21973.

Chua, J.Y., Pendharkar, A.V., Wang, N., Choi, R., Andres, R.H., Gaeta, X., Zhang, J., Moseley, M.E., Guzman, R., 2011. Intra-arterial injection of neural stem cells using a microneedle technique does not cause microembolic strokes. J. Cereb. Blood Flow Metab. 31, 1263–1271. http://dx.doi.org/10.1038/jcbfm.2010.213.

Chung, E., Yamashita, H., Au, P., Tannous, B.A., Fukumura, D., Jain, R.K., 2009. Secreted Gaussia luciferase as a biomarker for monitoring tumor progression and treatment response of systemic metastases. PLoS One 4, e8316. http://dx.doi.org/10.1371/journal.pone.0008316.

Cole, S.W., Nagaraja, A.S., Lutgendorf, S.K., Green, P.A., Sood, A.K., 2015. Sympathetic nervous system regulation of the tumour microenvironment. Nat. Rev. Cancer 15, 563–572. http://dx.doi.org/10.1038/nrc3978.

Conley, F.K., 1979. Development of a metastatic brain tumor model in mice. Cancer Res. 39, 1001–1007.

Coussens, L.M., Werb, Z., 2002. Inflammation and cancer. Nature 420, 860–867. http://dx.doi.org/10.1038/nature01322.

Dalgleish, A.G., O'Byrne, K., 2006. Inflammation and Cancer. Springer, US. http://dx.doi.org/10.1007/0-387-26283-0_1, pp. 1–38.

Daphu, I., Sundstrøm, T., Horn, S., Huszthy, P.C., Niclou, S.P., Sakariassen, P.Ø., Immervoll, H., Miletic, H., Bjerkvig, R., Thorsen, F., 2013. In vivo animal models for studying brain metastasis: value and limitations. Clin. Exp. Metastasis 30, 695–710. http://dx.doi.org/10.1007/s10585-013-9566-9.

Degen, J.L., Palumbo, J.S., 2012. Hemostatic factors, innate immunity and malignancy. Thromb. Res. 129 (Suppl), S1–S5. http://dx.doi.org/10.1016/S0049-3848(12)70143-3.

DeWys, W.D., 1972. Studies correlating the growth rate of a tumor and its metastases and providing evidence for tumor-related systemic growth-retarding factors. Cancer Res. 32, 374–379.

Dhabhar, F.S., Malarkey, W.B., Neri, E., McEwen, B.S., 2012. Stress-induced redistribution of immune cells—From barracks to boulevards to battlefields: A tale of three hormones – Curt Richter Award Winner. Psychoneuroendocrinology 37, 1345–1368. http://dx.doi.org/10.1016/j.psyneuen.2012.05.008.

Do, J., Foster, D., Renier, C., Vogel, H., Rosenblum, S., Doyle, T.C., Tse, V., Wapnir, I., 2014. Ex vivo Evans blue assessment of the blood brain barrier in three breast cancer brain metastasis models. Breast Cancer Res. Treat. 144, 93–101. http://dx.doi.org/10.1007/s10549-014-2854-5.

Drew, P.J., Shih, A.Y., Driscoll, J.D., Knutsen, P.M., Blinder, P., Davalos, D., Akassoglou, K., Tsai, P.S., Kleinfeld, D., 2010. Chronic optical access through a polished and reinforced thinned skull. Nat. Methods 7, 981–984. http://dx.doi.org/10.1038/nmeth.1530.

Driscoll, J., Shih, A., Drew, P., Kleinfeld, D., 2011. Quantitative two-photon imaging of blood flow in cortex. Imaging Neurosci.

Du Four, S., Maenhout, S.K., De Pierre, K., Renmans, D., Niclou, S.P., Thielemans, K., Neyns, B., Aerts, J.L., 2015. Axitinib increases the infiltration of immune cells and reduces the suppressive capacity of monocytic MDSCs in an intracranial mouse melanoma model. Oncoimmunology 4, e998107. http://dx.doi.org/10.1080/2162402X.2014.998107.

Fidler, I.J., 2011. The role of the organ microenvironment in brain metastasis. Semin. Cancer Biol. 21, 107–112.

Figueiredo, G., Boll, H., Kramer, M., Groden, C., Brockmann, M.A., 2012. In vivo X-ray digital subtraction and CT angiography of the murine cerebrovasculature using an intra-arterial route of contrast injection. AJNR Am. J. Neuroradiol. 33, 1702–1709. http://dx.doi.org/10.3174/ajnr.A3071.

Glasner, A., Avraham, R., Rosenne, E., Benish, M., Zmora, O., Shemer, S., Meiboom, H., Ben-Eliyahu, S., 2010. Improving survival rates in two models of spontaneous postoperative metastasis in mice by combined administration of a beta-adrenergic antagonist and a cyclooxygenase-2 inhibitor. J. Immunol. 184, 2449–2457. http://dx.doi.org/10.4049/jimmunol.0903301.

Gotlieb, N., Rosenne, E., Matzner, P., Shaashua, L., Sorski, L., Ben-Eliyahu, S., 2015. The misleading nature of in vitro and ex vivo findings in studying the impact of stress hormones on NK cell cytotoxicity. Brain Behav. Immun. 45, 277–286. http://dx.doi.org/10.1016/j.bbi.2014.12.020.

Grimm, K.A., Tranquilli, W.J., Lamont, L.A., 2011. Essentials of Small Animal Anesthesia and Analgesia. John Wiley & Sons.

Grivennikov, S.I., Greten, F.R., Karin, M., 2010. Immunity, inflammation, and cancer. Cell 140, 883–899. http://dx.doi.org/10.1016/j.cell.2010.01.025.

Harris, N.R., Carter, P.R., Lee, S., Watts, M.N., Zhang, S., Grisham, M.B., 2010. Association between blood flow and inflammatory state in a T-cell transfer model of inflammatory bowel disease in mice. Inflamm. Bowel Dis. 16, 776–782. http://dx.doi.org/10.1002/ibd.21126.

Hattori, Y., Enmi, J., Kitamura, A., Yamamoto, Y., Saito, S., Takahashi, Y., Iguchi, S., Tsuji, M., Yamahara, K., Nagatsuka, K., Iida, H., Ihara, M., 2015. A novel mouse model of subcortical infarcts with dementia. J. Neurosci. 35, 3915–3928. http://dx.doi.org/10.1523/JNEUROSCI.3970-14.2015.

Hinton, C.V., Avraham, S., Avraham, H.K., 2010. Role of the CXCR4/CXCL12 signaling axis in breast cancer metastasis to the brain. Clin. Exp. Metastasis 27, 97–105. http://dx.doi.org/10.1007/s10585-008-9210-2.

Hori, K., Saito, S., Nihei, Y., Suzuki, M., Sato, Y., 1999. Antitumor effects due to irreversible stoppage of tumor tissue blood flow: evaluation of a novel combretastatin A-4 derivative, AC7700. Jpn. J. Cancer Res. 90, 1026–1038.

Horowitz, M., Neeman, E., Sharon, E., Ben-Eliyahu, S., 2015. Exploiting the critical perioperative period to improve long-term cancer outcomes. Nat. Rev. Clin. Oncol. 12, 213–226. http://dx.doi.org/10.1038/nrclinonc.2014.224.

Joyce, J.A., Pollard, J.W., 2009. Microenvironmental regulation of metastasis. Nat. Rev. Cancer 9, 239–252. http://dx.doi.org/10.1038/nrc2618.

Kaya, M., Ahishali, B., 2011. Assessment of permeability in barrier type of endothelium in brain using tracers: Evans blue, sodium fluorescein, and horseradish peroxidase. Methods Mol. Biol. 763, 369–382. http://dx.doi.org/10.1007/978-1-61779-191-8_25.

Kienast, Y., Winkler, F., 2010. Therapy and prophylaxis of brain metastases. Expert Rev. Anticancer Ther. 10, 1763–1777. http://dx.doi.org/10.1586/era.10.165.

Kienast, Y., von Baumgarten, L., Fuhrmann, M., Klinkert, W.E.F., Goldbrunner, R., Herms, J., Winkler, F., 2010. Real-time imaging reveals the single steps of brain metastasis formation. Nat. Med. 16, 116–122. http://dx.doi.org/10.1038/nm.2072.

Kirnö, K., Friberg, P., Grzegorczyk, A., Milocco, I., Ricksten, S.E., Lundin, S., 1994. Thoracic epidural anesthesia during coronary artery bypass surgery: effects on cardiac sympathetic activity, myocardial blood flow and metabolism, and central hemodynamics. Anesth. Analg. 79, 1075–1081.

Kraft, P., Schwarz, T., Göb, E., Heydenreich, N., Brede, M., Meuth, S.G., Kleinschnitz, C., 2013. The phosphodiesterase-4 inhibitor rolipram protects from ischemic stroke in mice by reducing blood-brain-barrier damage, inflammation and thrombosis. Exp. Neurol. 247, 80–90. http://dx.doi.org/10.1016/j.expneurol.2013.03.026.

Lee, B.-C., Lee, T.-H., Avraham, S., Avraham, H.K., 2004a. Involvement of the chemokine receptor CXCR4 and its ligand stromal cell-derived factor 1alpha in breast cancer cell migration through human brain microvascular endothelial cells. Mol. Cancer Res. 2, 327–338.

Lee, J.S., Lee, D.S., Kim, Y.K., Kim, J., Lee, H.Y., Lee, S.K., Chung, J.-K., Lee, M.C., 2004b. Probabilistic map of blood flow distribution in the brain from the internal carotid artery. Neuroimage 23, 1422–1431. http://dx.doi.org/10.1016/j.neuroimage.2004.07.057.

Li, Z., Liang, G., Ma, T., Li, J., Wang, P., Liu, L., Yu, B., Liu, Y., Xue, Y., 2015. Blood-brain barrier permeability change and regulation mechanism after subarachnoid hemorrhage. Metab. Brain Dis. 30, 597–603. http://dx.doi.org/10.1007/s11011-014-9609-1.

Liu, J., Wang, P., Zhang, X., Zhang, W., Gu, G., 2014. Effects of different concentration and duration time of isoflurane on acute and long-term neurocognitive function of young adult C57BL/6 mouse. Int. J. Clin. Exp. Pathol. 7, 5828–5836.

Lorger, M., Felding-Habermann, B., 2010. Capturing changes in the brain microenvironment during initial steps of breast cancer brain metastasis. Am. J. Pathol. 176, 2958–2971. http://dx.doi.org/10.2353/ajpath.2010.090838.

Lu, T.-S., Avraham, H.K., Seng, S., Tachado, S.D., Koziel, H., Makriyannis, A., Avraham, S., 2008. Cannabinoids inhibit HIV-1 Gp120-mediated insults in brain microvascular endothelial cells. J. Immunol. 181, 6406–6416.

Machinami, R., 1973. A study of the invasive growth of malignant tumors. II. Ultrastructural features of the metastatic growth of Yoshida ascites hepatoma 7974 in the rat brain. Acta Pathol. Jpn. 23, 261–278.

Manaenko, A., Chen, H., Kammer, J., Zhang, J.H., Tang, J., 2011. Comparison Evans Blue injection routes: intravenous versus intraperitoneal, for measurement of blood-brain barrier in a mice hemorrhage model. J. Neurosci. Methods 195, 206–210. http://dx.doi.org/10.1016/j.jneumeth.2010.12.013.

Melamed, R., Rosenne, E., Shakhar, K., Schwartz, Y., Abudarham, N., Ben-Eliyahu, S., 2005. Marginating pulmonary-NK activity and resistance to experimental tumor metastasis: suppression by surgery and the prophylactic use of a β-adrenergic antagonist and a prostaglandin synthesis inhibitor. Brain Behav. Immun. 19, 114–126. http://dx.doi.org/10.1016/j.bbi.2004.07.004.

Melamed, R., Rosenne, E., Benish, M., Goldfarb, Y., Levi, B., Ben-Eliyahu, S., 2010. The marginating-pulmonary immune compartment in rats: characteristics of continuous inflammation and activated NK cells. J. Immunother. 33, 16–29. http://dx.doi.org/10.1097/CJI.0b013e3181b0b146.

Melillo, G., 2011. Hypoxia: jump-starting inflammation. Blood, 117.

Middlekauff, H.R., Nguyen, A.H., Negrao, C.E., Nitzsche, E.U., Hoh, C.K., Natterson, B. A., Hamilton, M.A., Fonarow, G.C., Hage, A., Moriguchi, J.D., 1997. Impact of acute mental stress on sympathetic nerve activity and regional blood flow in advanced heart failure: implications for 'triggering' adverse cardiac events. Circulation 96, 1835–1842. http://dx.doi.org/10.1161/01.CIR.96.6.1835.

Nguyen, Q.-T., Driscoll, J., Dolnick, E.M., Kleinfeld, D., 2009. MPScope 2.0: A computer system for two-photon laser scanning microscopy with concurrent plasma-mediated ablation and electrophysiology. In: Frostig, R.D. (Ed.), In Vivo Optical Imaging of Brain Function (second ed.) Boca Raton (FL): CRC Press/Taylor & Francis (Chapter 4).

Pein, M., Oskarsson, T., 2015. Microenvironment in metastasis: roadblocks and supportive niches. Am. J. Physiol. Cell Physiol. 309, C627–C638. http://dx.doi.org/10.1152/ajpcell.00145.2015.

Preusser, M., Capper, D., Ilhan-Mutlu, A., Berghoff, A.S., Birner, P., Bartsch, R., Marosi, C., Zielinski, C., Mehta, M.P., Winkler, F., Wick, W., von Deimling, A., 2012. Brain metastases: pathobiology and emerging targeted therapies. Acta Neuropathol. 123, 205–222. http://dx.doi.org/10.1007/s00401-011-0933-9.

Quail, D.F., Joyce, J.A., 2013. Microenvironmental regulation of tumor progression and metastasis. Nat. Med. 19, 1423–1437. http://dx.doi.org/10.1038/nm.3394.

Rozniecki, J.J., Sahagian, G.G., Kempuraj, D., Tao, K., Jocobson, S., Zhang, B., Theoharides, T.C., 2010. Brain metastases of mouse mammary adenocarcinoma is increased by acute stress. Brain Res. 1366, 204–210. http://dx.doi.org/10.1016/j.brainres.2010.09.085.

Sawchenko, P., Swanson, L., 1981. Central noradrenergic pathways for the integration of hypothalamic neuroendocrine and autonomic responses. Science 214, 685–687. http://dx.doi.org/10.1126/science.7292008 (80-).

Schackert, G., Price, J.E., Bucana, C.D., Fidler, I.J., 1989. Unique patterns of brain metastasis produced by different human carcinomas in athymic nude mice. Int. J. Cancer 44, 892–897.

Semenza, G.L., 2009. Regulation of oxygen homeostasis by hypoxia-inducible factor. Physiology, 24.

Shih, A.Y., Driscoll, J.D., Drew, P.J., Nishimura, N., Schaffer, C.B., Kleinfeld, D., 2012. Two-photon microscopy as a tool to study blood flow and neurovascular coupling in the rodent brain. J. Cereb. Blood Flow Metab. 32, 1277–1309. http://dx.doi.org/10.1038/jcbfm.2011.196.

Silasi, G., She, J., Boyd, J.D., Xue, S., Murphy, T.H., 2015. A mouse model of small-vessel disease that produces brain-wide-identified microocclusions and regionally selective neuronal injury. J. Cereb. Blood Flow Metab. 35, 734–738. http://dx.doi.org/10.1038/jcbfm.2015.8.

Song, H.-T., Jordan, E.K., Lewis, B.K., Liu, W., Ganjei, J., Klaunberg, B., Despres, D., Palmieri, D., Frank, J.A., 2009. Rat model of metastatic breast cancer monitored by MRI at 3 T and bioluminescence imaging with histological correlation. J. Transl. Med. 7, 88. http://dx.doi.org/10.1186/1479-5876-7-88.

Sperduto, P.W., Chao, S.T., Sneed, P.K., Luo, X., Suh, J., Roberge, D., Bhatt, A., Jensen, A. W., Brown, P.D., Shih, H., Kirkpatrick, J., Schwer, A., Gaspar, L.E., Fiveash, J.B., Chiang, V., Knisely, J., Sperduto, C.M., Mehta, M., 2010. Diagnosis-specific prognostic factors, indexes, and treatment outcomes for patients with newly diagnosed brain metastases: a multi-institutional analysis of 4,259 patients. Int. J. Radiat. Oncol. Biol. Phys. 77, 655–661. http://dx.doi.org/10.1016/j.ijrobp.2009.08.025.

Strell, C., Entschladen, F., 2008. Extravasation of leukocytes in comparison to tumor cells. Cell Commun. Signal. 6, 10. http://dx.doi.org/10.1186/1478-811X-6-10.

Sullivan, M.J., Knight, J.D., Higginbotham, M.B., Cobb, F.R., 1989. Relation between central and peripheral hemodynamics during exercise in patients with chronic heart failure. Muscle blood flow is reduced with maintenance of arterial perfusion pressure. Circulation 80, 769–781. http://dx.doi.org/10.1161/01.CIR.80.4.769.

Taveras, J.M., Mount, L.A., Friedenberg, R.M., 1954. Arteriographic demonstration of external-internal carotid anastomosis through the ophthalmic arteries. Radiology 63, 525–530. http://dx.doi.org/10.1148/63.4.525.

Theoharides, T.C., Rozniecki, J.J., Sahagian, G., Jocobson, S., Kempuraj, D., Conti, P., Kalogeromitros, D., 2008. Impact of stress and mast cells on brain metastases. J. Neuroimmunol. 205, 1–7. http://dx.doi.org/10.1016/j.jneuroim.2008.09.014.

Ushio, Y., Chernik, N.L., Shapiro, W.R., Posner, J.B., 1977. Metastatic tumor of the brain: development of an experimental model. Ann. Neurol. 2, 20–29. http://dx.doi.org/10.1002/ana.410020104.

Veltkamp, R., Siebing, D.A., Sun, L., Heiland, S., Bieber, K., Marti, H.H., Nagel, S., Schwab, S., Schwaninger, M., 2005. Hyperbaric oxygen reduces blood-brain barrier damage and edema after transient focal cerebral ischemia. Stroke 36, 1679–1683. http://dx.doi.org/10.1161/01.STR.0000173408.94728.79.

Wilde, D.W., Massey, K.D., Walker, G.K., Vollmer, A., Grekin, R.J., 2000. High-fat diet elevates blood pressure and cerebrovascular muscle Ca2+ current. Hypertension 35, 832–837. http://dx.doi.org/10.1161/01.HYP.35.3.832.

Wolff, G., Davidson, S.J., Wrobel, J.K., Toborek, M., 2015. Exercise maintains blood-brain barrier integrity during early stages of brain metastasis formation. Biochem. Biophys. Res. Commun. http://dx.doi.org/10.1016/j.bbrc.2015.04.153.

Wu, Y., Zhou, B.P., 2009. Inflammation: a driving force speeds cancer metastasis. Cell Cycle 8, 3267–3273. http://dx.doi.org/10.4161/cc.8.20.9699.

Yoshida, K., Ogasawara, K., Saura, H., Saito, H., Kobayashi, M., Yoshida, K., Terasaki, K., Fujiwara, S., Ogawa, A., 2015. Post-carotid endarterectomy changes in cerebral glucose metabolism on (18)F-fluorodeoxyglucose positron emission tomography associated with postoperative improvement or impairment in cognitive function. J. Neurosurg. 1–9. http://dx.doi.org/10.3171/2014.12.JNS142339.

Zhang, C., Yu, D., 2011. Microenvironment determinants of brain metastasis. Cell Biosci. 1, 8. http://dx.doi.org/10.1186/2045-3701-1-8.